Effects of Molecular Association on Polarizability Relaxation in Liquid Mixtures of Benzene and Hexafluorobenzene

M. Dolores Elola* and Branka M. Ladanyi*

Department of Chemistry, Colorado State University, Fort Collins, Colorado 80523

Alessandra Scodinu, Brian J. Loughnane, and John T. Fourkas*,†

Eugene F. Merkert Chemistry Center, Boston College, Chestnut Hill, Massachusetts 02467

Received: August 22, 2005; In Final Form: October 13, 2005

In this work we have studied the relaxation dynamics of the many-body polarizability anisotropy in liquid mixtures of benzene (Bz) and hexafluorobenzene (Hf) at room temperature by femtosecond optical heterodyne-detected Raman-induced Kerr effect spectroscopy (OHD-RIKES) experiments and molecular dynamics (MD) simulations. The computed polarizability response arising from intermolecular interactions was included using the first-order dipole−induced-dipole model with the molecular polarizability distributed over the carbon sites of each molecule. We found good qualitative agreement between experiments and simulations in the features exhibited by the nuclear response function $R(t)$ for pure liquids and mixtures. The long-time diffusive decay of $R(t)$ was observed to vary substantially with composition, slowing down noticeably with dilution of each of the species as compared with that in the corresponding pure liquids. MD simulation shows that the effect on $R(t)$ is due to the formation of strong and localized intermolecular association between Bz and Hf species that hinder the rotational diffusive dynamics. The formation of these Bz−Hf complexes in the liquid mixtures also modifies the rotational diffusive dynamics of the component species in such a way that cannot be explained solely in terms of a viscosity effect. Even though the computed orientational diffusive relaxation times associated with Bz and Hf are larger by a factor of ∼2 than those from experiments, we found similar trends in experiments and simulations for these characteristic times as a function of composition. Namely, the collective and single-molecule orientational correlation times associated with Bz are observed to grow monotonically with the dilution of Bz, while those corresponding to Hf species exhibit a maximum at the equimolar composition. We attribute the quantitative discrepancy between experiments and simulations to the use of the Williams potential, which seems to overestimate the intermolecular interactions and thus predicts not only a slower translational dynamics but also a slower rotational diffusion dynamics than in real fluids.

1. Introduction

The formation of a solid upon mixing hexafluorobenzene (Hf) and benzene (Bz) was first observed by Patrick and Prosser[1] nearly half a century ago. They reported a maximum in the melting temperature vs composition diagram of 23.7 °C, corresponding to the equimolar mixture of two substances; while the melting points of the pure components, benzene and hexafluorobenzene, are about 18 °C below that temperature, corresponding to 5.4 and 5.0 °C, respectively. Crystallographic and X-ray investigations revealed that the structure of the Bz/Hf solid compound was composed of columns of alternating Hf−Bz molecules in parallel stacks.[2] Whereas in the pure-component solids, the quadrupole moments of like polarity interact to give a solid composed of slipped parallel and perpendicular ordered pairs of molecules, in the Bz/Hf solid compound the opposite polarity of the quadrupoles produces stacked chains of alternating Bz and Hf molecules.[3] In the liquid phase, the long-range structural order found for the Bz/Hf solid is largely lost. However, thermodynamic[4] and X-ray diffraction studies[5,6] support the existence of the 1:1 interspecies complex in liquid binary mixtures at room temperature.

Intermolecular dynamics for molecular liquids occur in the far IR, terahertz frequency range. This spectral region of various liquids has been probed using light-scattering techniques and far IR absorption methods. However, even though spectroscopic measurements on Bz/Hf liquid mixtures have provided indirect support for complex formation, this evidence has not been conclusive in view of the difficulties of identifying its contributions to the experimental observables.

Perhaps the most clear-cut signature of a significant effect of intermolecular interactions on liquid dynamics is the observation of nonadditivity in ultrafast spectroscopic data, i.e., the impossibility of fitting the total spectral density of the solution by the weighted sum of its components.[7] This method was originally applied by Chang and Castner to their study of formamide−water and formamide−acetonitrile mixtures, in which dilution was found to have a significant effect on intermolecular correlations, reflected in the dramatic changes observed in the librational response.

Tassaing et al.[9] applied the same method to far IR spectra of equimolar liquid mixtures formed by Bz and Hf, finding a marked deviation from additivity in the difference spectrum which exhibits a well-defined band at about 33 cm^{-1}. This result was interpreted by the authors as evidence for the existence of strong local ordering, and interpreted as the signature of complexes with lifetimes of the order of a picosecond in the

* Corresponding authors. E-mail: dolores@colostate.edu; Branka.Ladanyi@colostate.edu; fourkas@umd.edu

† Current address: Department of Chemistry and Biochemistry, University of Maryland, College Park, MD 20742.

10.1021/jp054733n CCC: $30.25
Published on Web 11/23/2005

liquid state. It is worth noting, however, that far IR spectra are strongly attenuated at low frequencies with the consequence that long time scales, above ≈10 ps (which correspond to frequencies below ≈3 cm^{-1}), are not in general accessible from these measurements. Since the IR spectra studied by Tassaing et al. were reported for frequencies above 15 cm^{-1}, they were able to analyze dynamical effects that take place only for time scales below 2 ps.

Femtosecond optical heterodyne-detected Raman-induced Kerr effect spectroscopy (OHD-RIKES) techniques have demonstrated to be a very powerful tool for investigating far IR molecular dynamics, because they are able to probe the low frequency intermolecular part of the spectrum with a good signal-to-noise ratio. Neelakandan et al.[10] observed nonadditivity in the optical Kerr effect (OKE) response of binary mixtures of benzene and hexafluorobenzene using OHD-RIKES. For the range of compositions studied; they found the largest deviations occurring as the mole fraction approached the equimolar mixture. They analyzed the long-time portion (>2 ps) of the OHD-RIKES data for the mixtures by a multiexponential fit, and they did not find any component with a reorientation time that was slower than that associated to the monomers. However, the limited signal-to-noise ratio of the data in this study precluded access to the OHD-RIKES transients at times greater than 10 ps, potentially masking longer relaxation components.

Raman line widths have been measured at room temperature for pure benzene and hexafluorobenzene and their binary mixtures by Tanabe and Hirashi.[11] Their study provides indirect support for complex formation, revealing a strong hindrance of the single-molecule reorientational tumbling molecular motions in these mixtures that cannot be explained in terms of viscosity effects.

The OKE spectrum of pure liquid benzene has been previously studied by MD simulations by Chelli et al.,[12] and more recently by Ryu and Stratt.[13] The results obtained by Chelli and co-workers indicate that the relaxation of the local structures around a molecule is the main source of dephasing in benzene. The authors state that this relaxation mechanism is responsible for the dephasing of the low frequency tumbling librations giving rise to the intermediate quasi-exponential relaxation observed in OKE experiments. Ryu and Stratt[13] explored the OKE spectrum of benzene by MD simulation and instantaneous normal mode (INM) analysis. By separating the responses arising from rotational and translational degrees of freedom, they showed that the unusual shape of the experimental benzene OKE spectra, also common to other aromatic molecules[14−19] (i.e., exhibiting a flat region at intermediate frequencies), arises from the presence of an especially large ratio of rotational to translational bandwidths. The large rotational bandwidth is due, in turn, to the planarity of the molecules, which requires that the moment of inertia for spinning is the sum of tumbling moments of inertia.

Cabaço et al.[6] studied the local structure in Bz/Hf liquid mixtures by MD simulations, and in agreement with their neutron diffraction experiments, they found a strong structural enhancement upon mixing Bz and Hf, due to the formation of well defined heterodimers in a quasistacked configuration. Two of us have also recently studied the structure and dynamics in these mixtures,[20] finding evidence for the existence of Bz−Hf heterodimers in the liquid phase based on the results obtained for the radial-angular pair correlation functions, velocity cross correlations, and average lifetimes of the complexes. The estimations obtained for the lifetimes associated with Bz−Hf pairs in solution were found to depend strongly on the scheme chosen to compute the characteristic times, but they actually correspond to relatively long-lived entities, lying in the range 30−40 ps from direct averaging schemes and around 60−120 ps from autocorrelation methods.

In this work we study the dynamics of Bz/Hf liquid binary mixtures using both new OHD-RIKES data that extend to long times and detailed molecular dynamics simulations. Our goal is to elucidate aspects of the microscopic intermolecular structure and dynamics of Bz/Hf mixtures that to date have remained obscure.

The remainder of this article is organized as follows: In section II we present the experimental details. In section III we summarize the definitions needed in the calculation of the OKE response in time and frequency domains for a binary mixture. In section IV the details of the simulation and the model potential used are reported, and a description of the distributed site polarizability model for the interaction-induced polarizability is given. The results for the OKE response functions, time correlation functions, and spectra are presented and discussed in section V. A direct comparison between experiment and simulation is made for several mixture compositions. Finally we conclude in section VI with the summary of our main findings.

II. Experimental Section

All experiments were performed at a temperature of 298 K. Both benzene and hexafluorobenzene were distilled before use. Once a given mixture was prepared, a sample was immediately placed in a 1 mm path length cuvette that was capped with a Teflon stopper and sealed with vacuum epoxy to prevent leakage. If a new sample was required at a given mole fraction, a fresh mixture was prepared to ensure that the proportions were exact. In addition to neat benzene and hexafluorobenzene, samples with benzene mole fractions of 0.05, 0.10, 0.15, 0.20, 0.25, 0.30, 0.35, 0.40, 0.60, 0.70, 0.80, and 0.90 were studied.

The OHD-RIKES experimental setup and data collection procedures were identical to those reported previously.[21] To maximize the signal-to-noise ratio of the data, several scans were taken for each mixture at positive and negative heterodyne angles. The difference between the two scans yields the heterodyne contribution to the OHD-RIKES signal.

To fit our data with the greatest possible accuracy, we employed an integration procedure that we introduced previously.[22] The OHD-RIKES signal is the negative time derivative of the depolarized component of the many-body polarizability correlation function of the liquid, $\psi_{xz}^{MM}(t)$. This correlation function can be obtained by numerical integration of the heterodyne contribution of the OHD-RIKES signal. Fitting integrated data has two major advantages over working with the OHD-RIKES decays directly. First, integration removes high-frequency noise from the data, providing a significantly smoother curve for fitting. Second, it is immediately clear, upon visual inspection of integrated data, at what time the data become too noisy to include in a fit. However, this procedure also requires that the constant of integration be determined, adding an additional parameter to any fitting function. So long as the long-time behavior of the decay has a known functional form, such as an exponential in the case of the decays reported here, determination of the constant of integration is generally straightforward. Indeed, it is often necessary to employ such a parameter in the fitting of unintegrated data that extend out to long delay times in order to set the baseline for the fits as accurately as possible.

All fits of the integrated data were performed using a commercial nonlinear least squares routine (SigmaPlot 9.0). For high mole fractions of benzene, the data were fit, at times of 5

ps and greater, to the sum of two exponentials, for a total of five fitting parameters (two amplitudes, two decay constants, and the constant of integration). At these mole fractions unique fits were obtained. At lower mole fractions of benzene, the so-called intermediate response[23,24] became strong enough and long enough in time scale to necessitate the use of three exponentials in the fits, although only the slowest two, which correspond to orientational diffusion, are reported below. In addition, the time scales of the two slowest exponentials in some cases were close enough to one another that fits were not unique, and so additional constraints were employed (vide infra).

Once the fitting parameters for the integrated decays had been determined, they were used to strip long-time tails onto the heterodyne components of the OHD-RIKES decays in order to improve the frequency resolution of the final spectra. The Fourier transform deconvolution procedure of McMorrow and Lotshaw[25,26] was then used to obtain the OKE spectra corresponding to the OHD-RIKES decays. Reduced spectral densities were obtained by removing the orientational decays from the deconvolved response functions and then transforming into the frequency domain. An exponential rise with a time constant of 200 fs was assumed for the orientational contribution to the response functions. This choice is somewhat arbitrary, but the exact value of this rise time does not have a significant effect on the shape of the reduced spectral density.

III. Theoretical Background

The many-body polarizability, Π, of a liquid composed of N optically anisotropic molecules is the relevant dynamical variable for various spectroscopic properties based on light scattering,

$$\boldsymbol{\Pi} = \boldsymbol{\Pi}^{\mathrm{M}} + \boldsymbol{\Pi}^{\mathrm{I}} \tag{1}$$

where the total polarizability has been expressed in terms of its molecular (intrinsic) $\boldsymbol{\Pi}^{\mathrm{M}}$ and induced $\boldsymbol{\Pi}^{\mathrm{I}}$ contributions. The first term is simply the sum of unperturbed gas-phase molecular polarizabilities $\boldsymbol{\alpha}_i$. For a system containing N molecules, the total molecular polarizability is given by

$$\boldsymbol{\Pi}^{\mathrm{M}} = \sum_{i}^{N} \boldsymbol{\alpha}_i \tag{2}$$

The second term in eq 1 arises from the interaction between the induced dipole on molecule j with the polarizability of the ith molecule. This interaction-induced contribution can be expressed, within the first-order dipole−induced-dipole (DID) approximation,[27−29] as follows:

$$\boldsymbol{\Pi}^{\mathrm{I}} \simeq \sum_{i}^{N} \sum_{j \neq i}^{N} \boldsymbol{\alpha}_i \cdot \mathbf{T}^{(2)}(\mathbf{r}_{ij}) \cdot \boldsymbol{\alpha}_j \tag{3}$$

where the interactions are implicitly assumed to involve one site (the center of mass) on each molecule. The above expression is based on the multipole expansion of molecular permanent and induced moments, with the result that interactions involve distances between molecular centers-of-mass. We refer to this approach as the center−center (CC) approximation. $\mathbf{T}^{(2)}(\mathbf{r}_{ij})$ is the dipole tensor that depends on the distance vector $\mathbf{r}_{ij} = \mathbf{r}_i - \mathbf{r}_j$ between molecules i and j. Its functional form in the case of a pair of ideal dipoles is

$$\mathbf{T}^{(2)}(\mathbf{r}) = \frac{3\hat{\mathbf{r}}\hat{\mathbf{r}} - \mathbf{1}}{r^3} \tag{4}$$

where $\hat{\mathbf{r}} = \mathbf{r}/r$ and $\mathbf{1}$ is the unit tensor. It can be demonstrated that when the distance r between the two polarizable sites i and j approaches a critical value ($\alpha_{\mathrm{crit}} = (4\bar{\alpha}_i\bar{\alpha}_j)^{1/6}$, where $\bar{\alpha}_i$ is the isotropic polarizability of site i), the polarization along the line connecting the two points goes to infinity and some components of $\boldsymbol{\Pi}^{\mathrm{I}}$ may become negative at shorter separations. Because the intermolecular separation between neighboring Bz and Hf molecules becomes short when arranged in a stacked face-to-face configuration,[6,20] we used a modified form of the dipole tensor given by Thole,[30] which avoids these unphysical divergencies in the polarization at short distances,

$$\mathbf{T}^{(2)}(\mathbf{r}) = \begin{cases} [3\hat{\mathbf{r}}\hat{\mathbf{r}}\, u^4 - (4u^3 - 3u^4)\,\mathbf{1}]/r^3 & \text{if } r \leq s \\ [3\hat{\mathbf{r}}\hat{\mathbf{r}} - \mathbf{1}]/r^3 & \text{if } r > s \end{cases} \tag{5}$$

where $s = a_s(\bar{\alpha}_i\bar{\alpha}_j)^{1/6}$. a_s represents the screening parameter for the length scale determined by the isotropic polarizabilities $(\bar{\alpha}_i\bar{\alpha}_j)^{1/6}$, and $u = r/s$. As in a previous work,[32] we have used the value of $a_s = 1.7278$ for the screening parameter, taken from ref 31.

The use of multipole expansion of intermolecular interactions becomes problematic when the distances between molecules are not necessarily larger than intramolecular distances. To avoid this problem, one can consider the molecular polarizability as distributed over a set of interacting sites within the molecule. In this case, the first-order contribution to the interaction-induced collective polarizability will thus be given by the expression

$$\boldsymbol{\Pi}^{\mathrm{I}} \simeq \sum_{i,\, j \neq i} \sum_{mn} \boldsymbol{\alpha}_{im} \cdot \mathbf{T}^{(2)}(\mathbf{r}_{im,jn}) \cdot \boldsymbol{\alpha}_{jn} \tag{6}$$

where now $\boldsymbol{\alpha}_{im}$ is the effective polarizability of site m on molecule i, and $\mathbf{r}_{im,jn}$ represents the distance between site m on molecule i and site n on molecule j. This approach will be referred to as the site−site (SS) approximation. Further details are given in section IV.

The dynamics of interest are given by the time correlation function (TCF) of an off-diagonal element of the many-body polarizability tensor,

$$\psi_{xz}(t) = \langle \Pi_{xz}(0)\Pi_{xz}(t) \rangle / \Gamma^2 \tag{7}$$

where Γ^2 is the depolarized light scattering intensity, i.e., $\psi_{xz}(0)$, of a noninteracting system containing the same number and types of molecules as the system of interest. For pure liquids composed of N rigid molecules, it is given by $\Gamma^2 = N\gamma^2/15$, with γ^2 the squared isolated-molecule polarizability anisotropy. When dealing with binary mixtures of species a and b, Γ^2 depends on a weighted sum of polarizability anisotropies of the two components: $\Gamma^2 = N(x_a\gamma_a{}^2 + x_b\gamma_b{}^2)/15$ where x_i represents the mole fraction and $\gamma_i{}^2$ the squared polarizability anisotropy of species $i = a, b$.

Inserting the expression (1) for the collective polarizability into $\psi_{xz}(t)$ (eq 7), the TCF can be separated into three contributions, namely MM, II and MI, the first two corresponding to molecular and induced polarizability autocorrelation and the third to their cross-correlation:

$$\psi_{xz}^{\mathrm{MM}}(t) = \langle \Pi_{xz}^{\mathrm{M}}(0)\Pi_{xz}^{\mathrm{M}}(t) \rangle / \Gamma^2$$

$$\psi_{xz}^{\mathrm{II}}(t) = \langle \Pi_{xz}^{\mathrm{I}}(0)\Pi_{xz}^{\mathrm{I}}(t) \rangle / \Gamma^2$$

$$\psi_{xz}^{\mathrm{MI}}(t) = \langle \Pi_{xz}^{\mathrm{M}}(0)\Pi_{xz}^{\mathrm{I}}(t) + \Pi_{xz}^{\mathrm{I}}(0)\Pi_{xz}^{\mathrm{M}}(t) \rangle / \Gamma^2 \tag{8}$$

In liquids modeled as composed by rigid molecules, the molecular polarizability $\mathbf{\Pi}^{M}$ may only fluctuate in time due to changes in the orientations of the molecules. The molecular contribution to the total TCF of collective polarizability anisotropy, explicitly written as

$$\psi_{xz}^{MM}(t) = \frac{1}{\Gamma^2}\sum_{i}^{N}\sum_{j}^{N}\langle \alpha_{i,xz}(0)\,\alpha_{j,xz}(t)\rangle \tag{9}$$

may be separated in turn into a single-molecule and a pair contribution,

$$\psi_{xz}^{MM}(t) = \psi_{xz}^{MMs}(t) + \psi_{xz}^{MMp}(t), \tag{10}$$

where $\psi_{xz}^{MMs}(t)$ is the single-molecule component, arising from terms with $i = j$, and $\psi_{xz}^{MMp}(t)$ is the pair (or distinct) contribution obtained from the remaining terms $[i \neq j]$ in the summation. Therefore, it might be interesting to investigate how much of $\psi_{xz}^{MM}(t)$ is due to single-molecule reorientations, and also to study the effect of the pair contribution on the decay rate of the total molecular TCF.

The polarizability of an isolated molecule of type a can be decomposed in its isotropic and anisotropic components, $\boldsymbol{\alpha}_i^a = \bar{\alpha}_a\mathbf{1} + \boldsymbol{\gamma}_i^a$, where $\bar{\alpha}_a = \mathrm{Tr}(\boldsymbol{\alpha}_i^a)/3$ is the component of rank $l = 0$ (isotropic) and $\boldsymbol{\gamma}_i^a$ represents the traceless component of rank $l = 2$ (anisotropic). For axially symmetric molecules, the molecular polarizability tensor has has two distinct components $\alpha_{a\parallel}$ and $\alpha_{a\perp}$, respectively parallel and perpendicular to the symmetry axis. $\boldsymbol{\gamma}_i^a$ can be expressed in the laboratory frame as

$$\boldsymbol{\gamma}_i^a = \left(\frac{2\Delta\alpha_a}{3}\right)\mathbf{Q}_i \tag{11}$$

where $\mathbf{Q}_i = [(3\hat{\mathbf{u}}_i\hat{\mathbf{u}}_i - \mathbf{1})/2]$ represents the orientational tensor, $\hat{\mathbf{u}}_i$ is the unit vector along the symmetry axis of molecule i and $\Delta\alpha_a = \alpha_{a\parallel} - \alpha_{a\perp}$, its molecular polarizability anisotropy. (Note that $(\Delta\alpha_a)^2 \equiv \gamma_a^2$, the scalar squared polarizability anisotropy). In the case of rigid symmetric-top molecules, $\psi_{xz}^{MM}(t)$ depends only on orientational correlations of the molecular axis, and in the case of liquid binary mixtures of species a and b, $\psi_{xz}^{MM}(t)$ will have contributions from like and unlike pairs of molecules,

$$\psi_{xz}^{MM}(t) = \psi_{aa}^{MM}(t) + \psi_{bb}^{MM}(t) + \psi_{ab}^{MM}(t) \tag{12}$$

where we have omitted the subscript xz in the case of the mixture component contributions for notational simplicity. In terms of molecular polarizabilities these are given by

$$\psi_{aa}^{MM}(t) = \frac{1}{\Gamma^2}\sum_{i}^{N_a}\sum_{j}^{N_a}\langle \alpha_{i,xz}^a(0)\alpha_{j,xz}^a(t)\rangle \tag{13}$$

(with an analogous expression for $\psi_{bb}^{MM}(t)$), and

$$\psi_{ab}^{MM}(t) = \frac{1}{\Gamma^2}\left[\sum_{i}^{N_a}\sum_{j}^{N_b}\left\langle \alpha_{i,xz}^a(0)\alpha_{j,xz}^b(t)\right\rangle + \sum_{i}^{N_a}\sum_{j}^{N_b}\left\langle \alpha_{i,xz}^a(t)\alpha_{j,xz}^b(0)\right\rangle\right] \tag{14}$$

For rigid, axially symmetric molecules we substitute eq 11 for the polarizability anisotropy into eqs 13 and 14. It can be demonstrated that the contribution from like pairs $\psi_{aa}^{MM}(t)$ to the molecular TCF $\psi_{xz}^{MM}(t)$, can be expressed as[27]

$$\psi_{aa}^{MM}(t) = \frac{\Gamma_a^2}{\Gamma^2}\left(\frac{1}{N_a}\sum_{i}^{N_a}\sum_{j}^{N_a}\langle P_2[\hat{\mathbf{u}}_i(0)\cdot\hat{\mathbf{u}}_j(t)]\rangle\right) \tag{15}$$

where $\Gamma_a^2 = N_a\gamma_a^2/15$ and $P_2(x)$ is the second-order Legendre polynomial. This function can be in turn written in terms of the corresponding single- and pair- contributions,

$$\psi_{aa}^{MM}(t) = \psi_{a}^{MMs}(t) + \psi_{aa}^{MMp}(t) \tag{16}$$

where

$$\psi_{a}^{MMs}(t) = \frac{\Gamma_a^2}{\Gamma^2}\left(\frac{1}{N_a}\sum_{i}^{N_a}\langle P_2[\hat{\mathbf{u}}_i(0)\cdot\hat{\mathbf{u}}_i(t)]\rangle\right) \tag{17}$$

Note, by the way, that the quantity in parentheses in the above expression is equal to one at $t = 0$, and thus the equivalent expression for $\psi_{aa}^{MMp}(0)$ (for $i \neq j$), modifies the initial unity value depending on the average orientational correlations among distinct molecules in the system; and second, in single-component liquids, eq 15 accounts for the total molecular contribution, and the value of the prefactor in eqs 15 and 17 is $\Gamma_a^2/\Gamma^2 \equiv 1$.

The function defined in eq 14 is already a purely pair contribution, since it originates from correlations of pairs of molecules of different species. Thus, we can write the identity $\psi_{ab}^{MM}(t) \equiv \psi_{ab}^{MMp}(t)$, and in terms of the Legendre polynomials,

$$\psi_{ab}^{MM}(t) = \left(\frac{\gamma_a\gamma_b/15}{\Gamma^2}\right)\sum_{i}^{N_a}\sum_{j}^{N_a}\Big[\langle P_2[\hat{\mathbf{u}}_i(0)\cdot\hat{\mathbf{u}}_j(t)]\rangle + \langle P_2[\hat{\mathbf{u}}_j(0)\cdot\hat{\mathbf{u}}_i(t)]\rangle\Big] \tag{18}$$

Since the spinning motions [rotations around the six-fold axis] do not change the polarizability of individual molecules, $\psi_{xz}^{MM}(t)$ only reflects the tumbling dynamics, i.e., the correlations among rotations of the molecules around the axes that lie in the molecular plane.

The OKE signal in the time domain provides information about the intermolecular dynamics through the nuclear response function $R(t)$, which is related to the time derivative of the polarizability anisotropy TCF by

$$R(t) = -\beta\frac{\partial}{\partial t}\psi_{xz}(t) \tag{19}$$

where $\beta = 1/k_BT$ is the usual Boltzmann factor. $R(t)$, like $\psi_{xz}(t)$ can be separated in turn into its molecular, interaction-induced, and cross contributions.

The nuclear response function can be represented in the frequency domain, by performing a Fourier-Laplace transform of the nuclear response according to

$$\chi(\omega) = \int_0^\infty e^{i\omega t}R(t)\,dt \tag{20}$$

where the imaginary part is the susceptibility, a spectral density for polarizability anisotropy relaxation,

$$\chi''(\omega) \equiv \mathrm{Im}[\chi(\omega)] = \int_0^\infty \sin(\omega t)R(t)\,dt \tag{21}$$

IV. Potentials and Simulation Details

The potential model we have chosen to describe the intermolecular interactions is the widely used Williams potential,[33,34]

TABLE 1: Intermolecular Potential Parameters[a]

pair	B_{mm} (kJ mol^{-1})	C_{mm} (Å^{-1})	A_{mm} (kJ mol^{-1} Å^6)	q_m/e
C−C	369 743	3.60	2 439.8	−0.153[b]
H−H	11 971	3.74	136.4	+0.120[c]
F−F	400 000	4.35	500.0	−0.120

[a] Reference 35. [b] For C atom in benzene. [c] For C atom in hexafluorobenzene.

in which the intermolecular potential energy between a pair of atoms is given by

$$U_{mn}(r) = B_{mn}\exp(-C_{mn}r) - \frac{A_{mn}}{r^6} + \frac{q_m q_n}{4\pi\epsilon_0 r} \qquad (22)$$

where m and n label the C, H, and F atoms and r is the distance between atoms m and n. Using this potential, each molecule was modeled as a rigid body with 12 interacting sites located on the atom positions. The first term in eq 22 accounts for short-range repulsion, the second term represents the attractive dispersive interactions, and the last term is the Coulombic electrostatic contribution, where q_m denotes the partial charge on site m. The values of the potential parameters were taken from ref 35, and are reproduced here in Table 1. Bond length distances were taken as $d_{C-C} = 1.393$ Å, $d_{C-H} = 1.027$ Å and $d_{C-F} = 1.320$ Å.

Cross potential parameters for the pure liquids were calculated from the usual combination rules, $B_{mn} = (B_{mm}B_{nn})^{1/2}$, $C_{mn} = (C_{mm} + C_{nn})/2$, and $A_{mn} = (A_{mm}A_{nn})^{1/2}$. However, the use of intermolecular cross parameters for interactions between atoms of unlike molecules computed from the standard combination rules leads to a pronounced overestimation of the internal energy of mixing, as already pointed out by others.[6,36] Song et al.[37] studied and tested the ability of the OPLS-AA models of alkanes and perfluoroalkanes to represent the unusual mixing behavior of alkane+perfluoroalkane systems.[37] They found that the failure of the geometric mean combining rule for reproducing the weaker-than-anticipated interactions between unlike molecules can be repaired by reducing the strength of cross H−F interactions by ∼25% relative to the geometric mean, obtaining in this way reasonable agreement with experiments. As in a previous work done by two of us,[20] and following the same spirit of Song et al., we have rescaled the H−F cross parameters to reduce the attraction and get weaker interactions, in the manner $A_{HF} = (1 - k_{HF})\sqrt{A_{HH}A_{FF}}$ and $C_{HF} = s_{HF}(C_{HH} + C_{FF})/2$. We found that the set of values $k_{HF} = 0.5$ and $s_{HF} = 0.952$ leads to a much better agreement between MD predictions and experiment.[20] This modification in the H−F site interactions implies a decrease of roughly 10% in the total molecular energy, consistent with previous works on hydrocarbon+fluorocarbon mixtures.[37,38]

In addition to the pure liquids, we have studied by MD simulations liquid mixtures with benzene mole fractions of $x_{Bz} = 0.2$, 0.5, and 0.8. As a first approach, we have calculated the densities of the simulated mixtures, assuming that they behave ideally, which implies considering the molar volumes as additive quantities. The excess volume of these mixtures has been measured at 313 K by Duncan et al.[39] They found that the excess volumes were always smaller than 1% of the ideal volume of the liquid. Thus, even though our simulations were done at room temperature (298 K), we presume that the estimation of the volumes of mixtures assuming ideality is reasonably justified by those experimental results.

The simulations were performed in the *NVE* ensemble at an average temperature of 298 K with a total of $N = 256$ rigid molecules placed in a cubic box corresponding to the ideal mixture density at that temperature, using component density values of 0.874 and 1.60 g/cm^3 for neat benzene and hexafluorobenzene, respectively.[12,40] Short-ranged intermolecular forces were cut off at half the box length, and Coulomb forces were treated via Ewald sums with conducting boundaries. The dynamics of the rigid planar molecules were based on the constraint method[41] to integrate the equations of motion. The Verlet algorithm[42,43] was used to integrate the equations of motion, with a time step of 5 fs, keeping the intramolecular distances between the basic set of atoms fixed by using the SHAKE iterative procedure.[44] Preliminary trajectories of 100 ps were run for equilibration at 298 K. After the equilibration period, the trajectories were saved and 2 ns runs were used for data analysis.

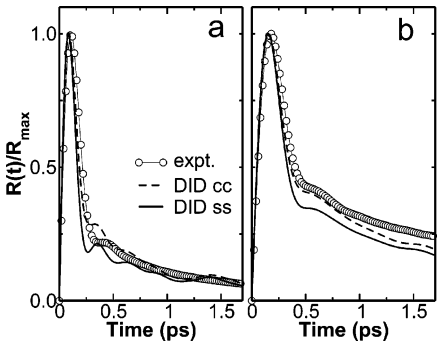

Figure 1. OKE nuclear response for (a) neat benzene and (b) hexafluorobenzene. Dashed and solid lines denote CC and SS models, respectively. Experimental response is plotted with circles.

Benzene and hexafluorobenzene are both symmetric-top molecules. Thus for both species the axes in which the polarizability tensor is diagonal are the same as the principal axes of inertia. The components of the isolated molecular polarizability tensor taken in this work were $\alpha_{||} = 6.54$ Å^3 and $\alpha_{\perp} = 11.73$ Å^3 for benzene (the subscripts || and ⊥ indicate parallel or perpendicular to the six-fold rotational symmetry axis respectively) and $\alpha_{||} = 4.58$ Å^3, $\alpha_{\perp} = 12.08$ Å^3 for hexafluorobenzene. These values in fact correspond to the following isotropic and anisotropic polarizabilities: $\bar{\alpha}_{Bz} = 10.00$ Å^3, $\Delta\alpha_{Bz} = -5.19$ Å^3, $\bar{\alpha}_{Hf} = 9.58$ Å^3 and $\Delta\alpha_{Hf} = -7.50$ Å^3.

So far we have not tried to use a complex scheme for the molecular polarizability model; we have considered instead the simple site−site scheme used previously by Mossa et al.[47] to investigate the Rayleigh spectra of supercooled liquid orthoterpenyl. Using this model, the molecular polarizability is distributed over the six carbon sites, with each of the sites being assigned 1/6 of the total molecular polarizability tensor. Thus the polarizability assigned to the mth carbon site of molecule i is given by

$$\boldsymbol{\alpha}_{im}^{\text{eff}} = \frac{\alpha_i}{6}\mathbf{1} + \frac{\gamma_i}{6} \quad (m = 1, 2,...6) \qquad (23)$$

The model assumes that the total molecular polarizability is a sum of these terms and neglects intramolecular-DID interactions.

V. Results

A. Pure Liquids: Comparison of Simulation with Experiments. Figure 1 shows a comparison between the simulated response functions, computed with both center−center (CC) and distributed site−site polarizabilities (SS) schemes, and the experimental OKE data of the pure liquids. We find good

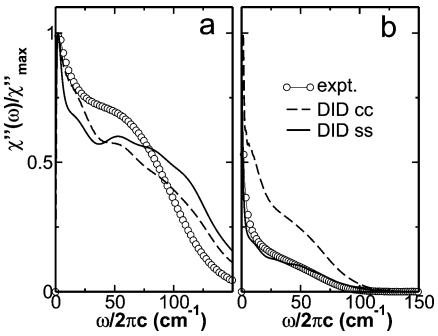

Figure 2. Low-frequency portion of OKE spectra for (a) neat benzene and (b) hexafluorobenzene.

agreement between experiment and theory for OKE response in both fluids.

In benzene, the computed nuclear response functions exhibit oscillations after the inertial peak that are more pronounced than in the real liquid. These oscillations are usually identified with cage effects that reverse the direction of molecular motions and give rise to negative regions in the molecular velocity autocorrelation functions,[27] as observed in liquid benzene[20,48] for molecular tumbling motions. The oscillations that appear in the simulated $R(t)$ functions, and that are much more damped in the experimental response, are indicative of a tendency for the Williams model potential to predict stiffer intermolecular interactions than in the real fluid. After 0.75 ps, CC and SS models yield similar intensities and agree with the experimental response.

In hexafluorobenzene, the amplitude of the nuclear response function seems to be underestimated by our calculations after the inertial peak by both polarizability models, CC and SS. In the time range depicted in Figure 1b, the CC model seems to predict nuclear response intensities in closer agreement with experiments. However, the slope of the decaying portion of $R(t)$ plays a very important role in determining the shape of the low-frequency spectral susceptibility. The much better agreement with experimental data can be appreciated in the frequency domain for hexafluorobenzene when using the SS model, as seen in Figure 2b. Figure 2 shows the OKE spectral susceptibilities, computed from both molecular models, along with the experimental spectra.

The two computed spectra in benzene (within CC and SS models) extend up to higher frequencies than the experimental spectrum, which extends roughly up to frequencies of about 200 cm^{-1}, due to the overestimation of the intermolecular interactions in the potential model. The use of CC or SS models for interaction-induced polarizabilities does not change this tendency very much.

The OKE spectra of liquids composed of aromatic molecules have been extensively studied by light scattering experiments.[14−17,49−54] It is well known that these spectra display analogous behaviors, namely, they exhibit flattened shapes at intermediate frequencies, falling off much more slowly to the low-frequency side than the spectra of liquids composed of linear molecules, such as CS_2. In particular, the existence of a flat region at intermediate frequencies in the low-frequency spectra at room temperature is a characteristic behavior exhibited in liquid benzene. Ryu and Stratt[13] analyzed the OKE spectrum of liquid benzene by MD simulations and INM theory and showed that the characteristic shape of the benzene spectrum is due in part to its molecular structure, i.e., the fact that it is a planar axially symmetric molecule, which means that its moments of inertia for tumbling and spinning are in the ratio

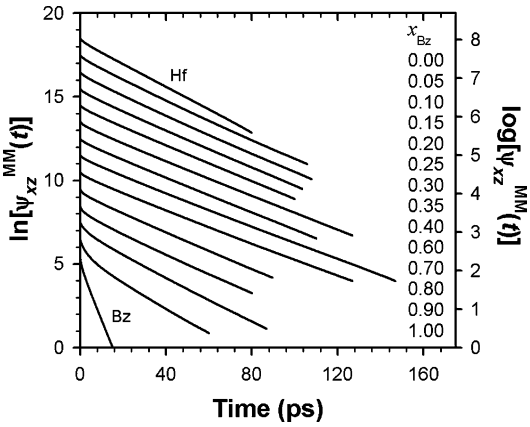

Figure 3. From top to bottom, experimental integrated OKE decays for the pure liquids and mixtures at various benzene mole fractions, as indicated in the panel. The data sets have been offset for clarity.

of 1:2. The peaks of the librational bands associated with the corresponding rotational motions determine the high and low ends of the flat regions, with translational and coupled translational-rotational dynamics filling in the intermediate region. Thus their explanation does not invoke specific dimer attractions to explain these spectra, as had been suggested earlier by others.[17] In our case, that unusual trend seems to be better described by the SS model than the CC approach, in which an almost monotonic decrease is observed in $\chi''(\omega)/\chi''_{max}$ with increasing frequency. We should note that Ryu and Stratt MD calculations are identical to our CC model results. Our computed OKE spectrum for benzene is in good agreement with previous calculations performed by Chelli et al.,[12] who have calculated the OKE spectrum of pure liquid benzene from MD simulations using two different intermolecular potentials, namely the Williams potential with a different set of parameters[55] and a LJ + Coulomb potential. They have also observed that both of their simulated spectra extend up to too high in frequencies, attributing this feature to a too stiff cage potential predicted by both potential models.

Distributing the polarizability over six molecular sites has a stronger positive impact on the OKE spectrum of Hf than of Bz. This is likely to be related to the different near-neighbor packing in the two liquids, with Hf exhibiting a stronger tendency toward parallel and Bz toward perpendicular orientations of the molecular planes,[20] making Hf more sensitive to the distribution of sites in the molecular plane. We also note that the overall agreement between the experimental and simulated $\chi''(\omega)/\chi''_{max}$ is significantly better for Hf than for Bz, suggesting that the intermolecular potential for Hf leads to a more accurate representation of liquid-state properties.

Since the distributed site−site polarizability scheme SS represents a more physically realistic model for the interaction induced polarizability and due to the closer agreement between computed SS and experimental OKE spectra, we only show and analyze in the following our results computed within the site−site model.

B. Binary Mixtures of Bz and Hf. *1. Optical Kerr Effect Decays.* Shown in Figure 3 are the experimental integrated OKE decays as a function of benzene mole fraction. These decays extend out an order of magnitude or more farther in time than those reported previously.[10] While the quantitative fitting of these data will be discussed below, a number of features are immediately apparent upon inspection. In all of the decays there is a component that decays roughly on the same time scale as the long-time decay in neat hexafluorobenzene. However, the

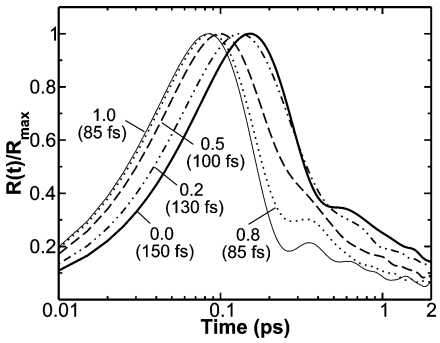

Figure 4. Normalized MD short-time nuclear response function of liquid mixtures, with benzene mole fraction (x_{Bz}) indicated and peak position in parentheses. Note the log scale on the horizontal axis, for a better visualization.

decay constant in all of the mixtures is greater than that for neat hexafluorobenzene, even at the highest benzene mole fractions. It is striking that the long-time decay is slower at a benzene mole fraction of 0.90 than in neat hexafluorobenzene, considering that the viscosity of benzene is approximately 30% lower than that of hexafluorobenzene at room temperature. Note also that the long-time decays become slower as a benzene mole fraction of 0.5 is approached from either direction. These observations are immediately suggestive of significant molecular association in the mixtures.

In Figure 4 the short-time inertial peak of the simulated, normalized nuclear response function is plotted for the whole range of compositions explored. Within 160 fs, the simulated nuclear response for benzene rapidly decays from the librational peak down to ~30% of the maximum amplitude, while the same decay (from maximum amplitude to ~40% of its value) takes roughly twice (345 fs) as long to attain in neat hexafluorobenzene. $R(t)$ evolves toward an intermediate response ($\approx$ 300−500 fs up to 2 ps) and then it gives rise to the diffusive regime. The oscillations modulating the decaying portion of the response (starting around 300 fs in benzene) diminish in amplitude in the Bz-rich mixture and at benzene concentrations $x_{Bz} = 0.2$ and 0.5. For pure hexafluorobenzene, damped oscillations can be seen again starting around 400 fs. The type of oscillations exhibited by $R(t)$ are often associated with hindered librational motions due to cage effects.[27,56,57]

Figure 5 shows the long-time tail of the total nuclear response, for all the compositions studied by MD, along with the experimental OKE responses for comparison. The computed functions are shown for times shorter than ~20 ps because they look rather noisy at longer time scales. Since the polarizability anisotropy TCF is a collective property, it converges very slowly; the long time portion of the time correlation functions are then less accurate, and the time derivative intensifies the magnitude of fluctuations. Consequently, that portion of the total TCFs [$t \gtrsim 20$ ps] was not taken into account for the fitting procedure. However, there is good qualitative agreement between the experimental and simulated curves, in particular in the time scale depicted in Figure 4, i.e., $0 \leq t \leq 20$ ps.

The experimental integrated OKE decays in Figure 3 are roughly biexponential at times of 5 ps and greater. Since the main contribution to $R(t)$ at long times comes basically from orientational dynamics,[13,27,29,32] it seems reasonable to identify the two exponentials with the orientational diffusion of the benzene and hexafluorobenzene species, respectively. However, from the point of view of the experiments, it is difficult to determine whether this interpretation is the appropriate or not. We know from theory that the molecular TCF, which reflects

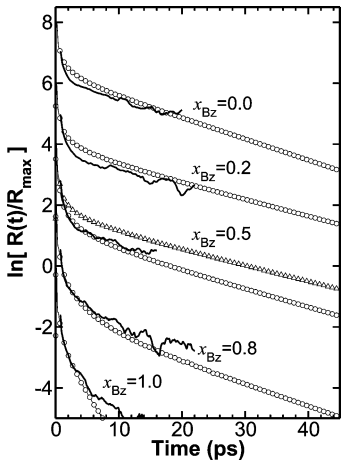

Figure 5. Logarithm of normalized OKE nuclear responses for liquid mixtures of different composition. Solid lines correspond to the simulated functions; experimental OKE signals are represented by circles. For the curves labeled with xBz = 0.5, circles and triangles correspond to experimental benzene mole fractions of 0.6 and 0.4, respectively. The decays have been offset for clarity.

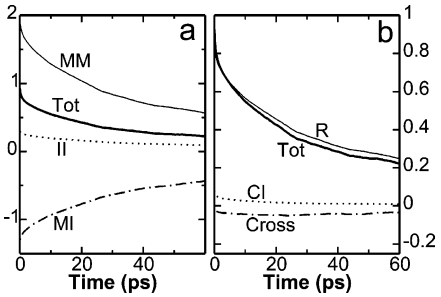

Figure 6. Contributions to the total polarizability ansiotropy TCF in (a) unprojected and (b) projected schemes (see text), for the equimolar mixture. Note the different scales on y-axis in the two panels.

the orientational relaxation of the collective polarizability anisotropy, is built up not only from the contributions arising from products between molecular polarizabilities of molecules of the same kind, $\psi_{aa}^{MM}(t) + \psi_{bb}^{MM}(t)$, but it has also a contributing term from the coupling between unlike molecules, $\psi_{ab}^{MM}(t)$ (see eq 12). In the absence of long-term association between the two species, orientational diffusion of the two species would be expected to lead to a biexponential decay.[58] However, this would not be expected to be the case here given the strong association between benzene and hexafluorobenzene. In the next section we investigate more deeply the decay rates and dependence on composition of the contributions to the collective molecular time correlation function, and we also compute the orientational correlation times arising from the simulated functions and compare them with values derived from fits of the experimental data.

The detailed comparison between experiments and theory in the next section will be done in terms of just the molecular (MM) component of the TCF arising from the simulations. This is because the main focus of the comparison will be on the relaxation times obtained from the fit of the longer-time experimental signal to a biexponential function. This portion of the decay is dominated by orientational diffusive dynamics. Before focusing on the MM portion of the MD response, we briefly examine the roles played by the portions of $\psi_{xz}(t)$ due to the interaction-induced polarizability. In Figure 6a we display the decomposition of $\psi_{xz}(t)$ for a typical mixture [$x_{Bz} = 0.5$] into its MM, MI, and II components. It can be seen that all three components are nonnegligible over the entire time interval

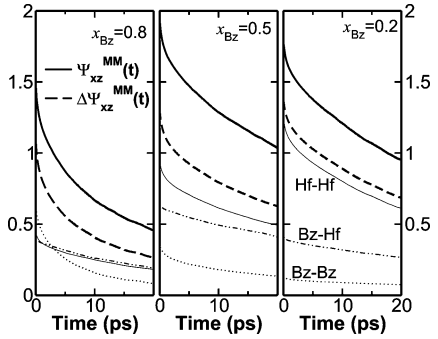

Figure 7. Total molecular TCF, $\psi_{xz}^{MM}(t)$ (thick solid lines) and the total TCF without the coupling term, $\Delta\psi_{xz}^{MM}(t) = [\psi_{xz}^{MM}(t) - \psi_{ab}^{MM}(t)]$ (thick dashed lines) for the three mixtures studied by MD. The mixture component contributions $\psi_{Bz-Bz}^{MM}(t)$ (···), $\psi_{Hf-Hf}^{MM}(t)$ (—), and $\psi_{Bz-Hf}^{MM}(t)$ (— ·· —) are also shown.

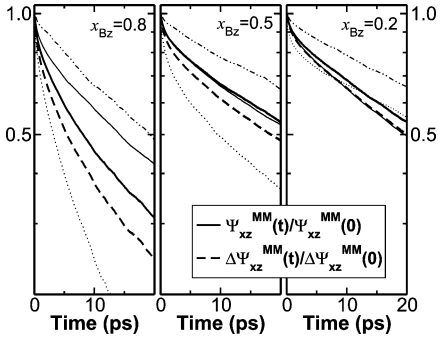

Figure 8. Same as Figure 7, but normalized to the initial value, and plotted on semilog scale.

displayed. In particular, $\psi_{xz}^{MI}(t)$, which is almost as large as $\psi_{xz}^{MM}(t)$, but of the opposite sign, decays at a similar rate as does $\psi_{xz}^{MM}(t)$ at long times. In fact, collective orientational relaxation is the main relaxation mechanism at long times. This can be made more evident by projecting Π_{xz}^{I} along Π_{xz}^{M}, a method that has been used and discussed in previous works.[27−29,32,59] The resulting polarizability components are then the reorientational (R) and collision-induced (CI) terms,

$$\Pi_{xz}^{R} = (1 + G_{xz})\Pi_{xz}^{M} \tag{24a}$$

$$\Pi_{xz}^{CI} = \Pi_{xz}^{I} - G_{xz}\Pi_{xz}^{M} \tag{24b}$$

where $G_{xz} = \langle \Pi_{xz}^{M} \Pi_{xz}^{I} \rangle / \langle (\Pi_{xz}^{M})^2 \rangle$. The decomposition of $\psi_{xz}(t)$ into the rotational and CI polarizability autocorrelations, $\psi_{xz}^{R}(t)$ and $\psi_{xz}^{CI}(t)$, and their cross-correlation, $\psi_{xz}^{Cross}(t)$, is depicted in Figure 6b. As can be seen from this figure, the intensities of $\psi_{xz}^{CI}(t)$ and $\psi_{xz}^{Cross}(t)$ are small compared to that of $\psi_{xz}^{R}(t)$. At times beyond approximately 10 ps, $\psi_{xz}^{R}(t)$ is clearly the dominant contribution to $\psi_{xz}(t)$. Thus on this time scale the main effect of interaction-induced contributions is to modify the intensity of the collective reorientation component through the constant scaling factor $[(1 + G_{xz})^2]$. Considering that $\psi_{xz}^{R}(t)$ and $\psi_{xz}(t)$ almost coincide on this time scale, it is reasonable to focus on the orientational component when comparing the diffusive relaxation portion of the OKE response to experiment.

2. Molecular Orientational Correlations. To investigate to what extent the molecular coupling term $\psi_{ab}^{MM}(t)$ modifies the intensity and the decay rate of the total molecular TCF, we have compared in Figure 7 the total MM function $\psi_{xz}^{MM}(t)$ (in thick solid lines) with the difference function $\Delta\psi_{xz}^{MM}(t) = \psi_{xz}^{MM}(t) - \psi_{ab}^{MM}(t)$ (in thick dashed lines) for the mixtures investigated.

Figure 7 displays a substantial positive contribution of the coupling term to the total intensity of the molecular TCF for all three mixtures, and this contribution is largest for the equimolar mixture. Figure 7 shows also the contributions from Bz−Bz, Hf−Hf and Bz−Hf correlations, with all three terms adding constructively to $\psi_{xz}^{MM}(t)$. We see that the coupling term $\psi_{Bz-Hf}^{MM}(t)$ decays with a rate similar to that of the slowest intraspecies component and remains important over the entire time scale depicted in Figure 7. Its intensity is larger than that of Bz−Bz correlations at all times in the $x_{Bz} = 0.2$ and $x_{Bz} = 0.5$ mixtures, while for the Bz-rich mixture, a similar situation occurs for times longer than ∼2.5 ps.

To investigate their contributions to the overall molecular relaxation rate, we display in Figure 8 the same curves normalized with their initial values.

By comparing the decay rates of $\psi_{xz}^{MM}(t)$ and $\psi_{ab}^{MM}(t)$, it is evident that the effect of the coupling term on the total molecular TCF is not just a constant positive shift in the amplitude but also a modification of the decay rate of $\psi_{xz}^{MM}(t)$, producing a slower decay, which is more pronounced as long as more Bz molecules are present in the mixture. The interspecies correlations represent the slowest relaxing component of $\psi_{xz}^{MM}(t)$ in the diffusive regime, but they also decay more slowly at short times, given that the inertial contribution is absent from $\psi_{ab}^{MM}(t)$ due to the lack of angular velocity cross-correlations at $t = 0$. In all three mixtures, the long-time decay rate of coupling term $\psi_{ab}^{MM}(t)/\psi_{ab}^{MM}(0)$ is similar to that of the more slowly decaying of the two intraspecies TCFs. In the equimolar mixture the decay rate of $\psi_{ab}^{MM}(t)$ resembles that of $\psi_{Hf-Hf}^{MM}(t)$, while in the other two mixtures it follows the minor intraspecies component. The fact that the decay rate of the molecular coupling between unlike molecules is close to that of the slower of the two intraspecies components suggests that it should be possible to fit the experimental decays to a sum of two exponentials. However, while the faster exponential can be attributed to a single species, the slower one should be attributed to the more slowly relaxing species plus the interspecies relaxation.

To quantify these features, the correlation times associated to each of the three contributions to $\psi_{xz}^{MM}(t)$ have been computed. The results are shown in Table 2 and they are discussed at the end of this section.

Next, we compare the decay rates of single-molecule and collective molecular polarizability anisotropy correlations between like species for both components, in pure liquids and mixtures, in Figure 9. The results for $\ln[\psi_{aa}^{MM}(t)/\psi_{aa}^{MM}(0)]$ are compared to those for the logarithm of the normalized single-molecule time correlation function, $\psi^{MMs}(t)/\psi^{MMs}(0)$, for each species.

As a common trend in Figure 9, we observe that collective molecular correlations (solid lines) decay always more slowly than the single-molecule TCFs (dashed lines), indicating that dynamical pair correlations are important. For both species the decay rates of collective and single-molecule molecular correlations become slower with the decrease of the corresponding mole fraction, indicating that interspecies interactions slow the reorientational diffusive dynamics. The difference in the decay rates of the collective and single-molecule correlations becomes progressively smaller with the addition of molecules of the other species into the mixture, consistent with increasing isolation of molecules of the same kind from each other. This is also likely to be an indirect consequence of association between benzene and hexafluorobenzene in the mixtures.

Figure 10 displays a direct comparison the normalized single-molecule polarizability TCFs $\psi^{MMs}(t)/\psi^{MMs}(0)$ at different benzene mole fractions.

TABLE 2: Collective and Single-Molecule Relaxation Times (in ps) Computed from MD Simulations

	Bz		Hf		Bz-Hf	τ_c^{aa}/τ_s^a	
x_{Bz}	τ_s^{Bz}	τ_c^{Bz-Bz}	τ_s^{Hf}	τ_c^{Hf-Hf}	τ_c^{Bz-Hf}	Bz	Hf
1.0	2.64	3.64				1.38	-
Expt.	2.71[a]	2.84[a]				1.05	-
		3.1[b]					
0.8	7.91	9.65	20.8	24.7	28.8	1.22	1.19
0.5	22.4	23.6	30.5	40.3	52.4	1.04	1.30
0.2	35.3	44.3	23.9	31.6	51.7	1.25	1.32
0.0			11.7	24.6			2.10
Expt.			10.6[c]	14.0[c]			1.32
				14.8[b]			

[a] Reference 24. [b] This work. [c] Reference 58.

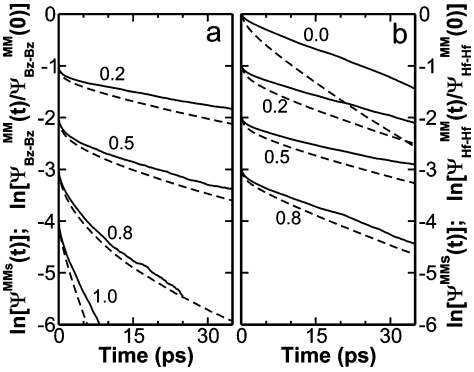

Figure 9. Logarithms of the normalized single-molecule (dashed lines) and collective like species molecular polarizability TCFs (solid lines) for (a) benzene and (b) hexafluorobenzene vs time in mixtures and pure liquids. The curves corresponding to $x_{Bz} = 0.2$, 0.5, 0.8, and 1.0 have been shifted vertically by -1, -2, -3, and -4, respectively. The numbers in the panels indicate the values of x_{Bz}.

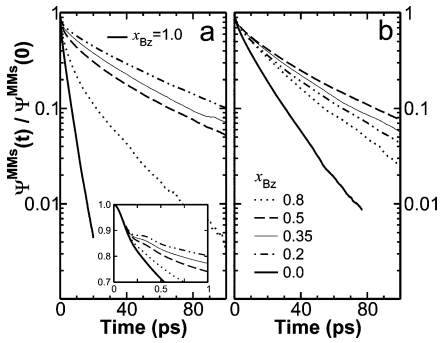

Figure 10. Normalized single-molecule orientational TCFs, $\psi^{MMs}(t)/\psi^{MMs}(0)$ for (a) benzene and (b) hexafluorobenzene molecules in mixtures, in semilog scale. The inset in panel (a) shows a detail of the short-time behavior in the time scale $0 \le t \le 1$ ps (linear scale).

The inset in panel (a) shows the short time behavior of $\psi^{MMs}(t)$ for Bz autocorrelations, where the change in the slope of the decay rate after the inflection point can be better appreciated. For symmetric-top molecules, the single-molecule correlation function, $\psi^{MMs}(t)$, can be expanded at short times in even powers of time, according to[60,61]

$$\psi^{MMs}(t) \approx 1 - \left(\frac{3k_BT}{I_\perp}\right)t^2 + \left(\frac{k_BT}{I_\perp}\right)^2 \times \left(17 - \frac{\xi}{1+\xi} + \frac{\langle N_\perp{}^2\rangle}{2(k_BT)^2}\right)\frac{t^4}{4} + \mathcal{O}(t^6) \quad (25)$$

where $\xi \equiv [(I_\perp/I_\parallel) - 1]$, being $I_\parallel$, $I_\perp$ the moments of inertia along and perpendicular to the symmetry axis respectively; and $\langle N_\perp{}^2\rangle$ stands for the mean square torque exerted on the symmetry axis of a molecule. The initial curvature (second moment) of these correlation functions depends only on the temperature and the moment of inertia, and not on intermolecular forces. Therefore, at very short times, when the contributions from the fourth moment are still negligible, the initial decays of $\psi^{MMs}(t)$ are the same for the whole range of compositions studied. However, at later times, the fourth moment starts making a substantial contribution to $\psi^{MMs}(t)$, and the higher level of hindrance in the rotational dynamics of individual molecules, as they associate strongly with neighbors of other species, manifests itself in the decrease of the decay rate with dilution, due to an increase in the mean square torque on the symmetry axis.

In the diffusive limit at long times, and assuming that the Debye theory of rotational relaxation is applicable, the rotational diffusion coefficients for tumbling dynamics, $D_\perp$, can be estimated from the long time decay of the single-molecule normalized function, $\psi^{MMs}(t)/\psi^{MMs}(0) \approx \exp(-6D_\perp t)$. Rotational diffusion coefficients for Bz and Hf in pure liquids and mixtures have been measured by Raman linewidth studies.[11,63] The experiments indicate that $D_\perp$ for the two species in the equimolar mixture are roughly half those in pure liquids, revealing a higher degree of hindrance of the tumbling motions in solution than in pure liquids. The change in $D_\perp$ for benzene with dilution is consistent with the increase in the viscosity of the system with the addition of hexafluorobenzene (which is a more viscous liquid than benzene). Nevertheless, the change is too large to be explained only in terms of a viscosity effect. Specifically, the viscosity of these mixtures decreases monotonically (but not linearly) as a function of mole fraction, from the value for pure Hf, $\eta_{Hf} = 0.87$ cP, to that corresponding to pure Bz, $\eta_{Bz} = 0.61$ cP. Thus, the decrease in $D_\perp$ for hexafluorobenzene with decreasing viscosity (higher benzene mole fraction) contradicts the predictions of hydrodynamic theories of orientational diffusion, according to which $D_\perp \propto 1/\eta$, where η is the viscosity of the system. This effect has then been attributed to the formation of an intermolecular association complex, which slows down the rotation of each species as its mole fraction in the mixture is lowered.[63] Our results from simulations agree with the experimental findings for the rotational diffusion coefficients. Our single-molecule TCFs display slower tumbling dynamics for both species in the equimolar mixture than in the pure liquids, as can be seen in Figure 10, but the changes observed in the slope of $\psi^{MMs}(t)/\psi^{MMs}(0)$ at long times are larger than those from experiments. Namely, the results of our simulations indicate that $D_\perp$ varies with dilution by a factor of $\sim$10 for benzene and $\sim$3 for hexafluorobenzene. This overestimation in the effect of slowing down the orientational diffusive dynamics in liquid mixtures is probably due to a deficiency in the model

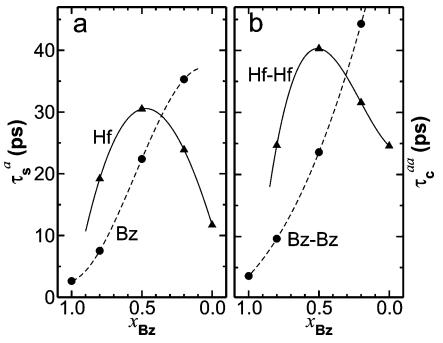

Figure 11. Single-molecule (a) and collective (b) orientational relaxation times for benzene (circles) and hexafluorobenzene (triangles) components in pure liquids and mixtures, as a function of the benzene mole fraction x_{Bz}. The lines are just guides to the eye.

Hamiltonian used in the simulations, which tends to predict stiffer intermolecular interactions.

The relaxation times associated to single-molecule and collective orientational correlations of polarizability anisotropy can be defined as the time integrals of the corresponding normalized TCFs, e.g.,

$$\tau_s^a = \int_0^\infty \psi_a^{\mathrm{MMs}}(t)/\psi_a^{\mathrm{MMs}}(0)\,\mathrm{d}t \tag{26}$$

and

$$\tau_c^{aa} = \int_0^\infty \psi_{aa}^{\mathrm{MM}}(t)/\psi_{aa}^{\mathrm{MM}}(0)\,\mathrm{d}t \tag{27}$$

Biexponential fits were used to calculate the contribution to the relaxation times in the diffusive regime, for $t > 2$ ps and $t > 5$ ps for single-molecule and collective orientational TCFs, respectively. The computed relaxation times for single-molecule and intraspecies molecular correlations are plotted in Figure 11 and reported in Table 2 along with the correlation time obtained for the coupling component $\psi_{ab}^{\mathrm{MM}}(t)$.

While single- and collective relaxation times for the Bz component increase monotonically with the addition of Hf into the mixture, a very different behavior is found for the Hf component: both relaxation times, τ_s^{Hf} and $\tau_c^{\mathrm{Hf-Hf}}$, have a maximum when the mole fractions of both components are equal. This behavior has already been anticipated in Figure 10b, where the slowest decay is observed to occur for $x_{Bz} = 0.5$.

As mentioned above, for some benzene mole fractions it is difficult to obtain unique fits to the integrated OKE data. However, we are able to use the simulation results in Figure 11 to give us guidance in developing constraints to assist in the fitting. We began by fitting the data for benzene mole fractions between 0.60 and 1; for these data it is possible to obtain robust biexponential fits. The faster decay time, which we can assume based on the above results reflects the benzene dynamics in this range of mole fractions, was found to vary linearly with mole fraction. We then made the assumption that this linear behavior would persist throughout all mole fractions of benzene. A linear least-squares fit to the benzene relaxation times for mole fractions between 0.60 and 1 was used to constrain the benzene relaxation time in nonlinear least-squares fits of the remaining data, yielding fits of high quality. The decay times from these fits are plotted in Figure 12. Although these data are not in quantitative agreement with the calculated values in Figure 11b, the degree of similarity between the calculated and experimental results is striking.

We can also obtain the relative amplitudes of the benzene and hexafluorobenzene components of the integrated OKE decays from the fits. In Figure 13 we plot these amplitudes as a function of benzene mole fraction. As can be seen from Figure 12, at a benzene mole fraction of 0.40 the two relaxation times are virtually identical, so it is not possible to determine the relative amplitudes for this mixture. In addition, based upon the simulation results discussed in this section, we assume that the amplitude of the slower decay component for any given mixture also contains the contribution of the coupling term $\psi_{ab}^{\mathrm{MM}}(t)$.

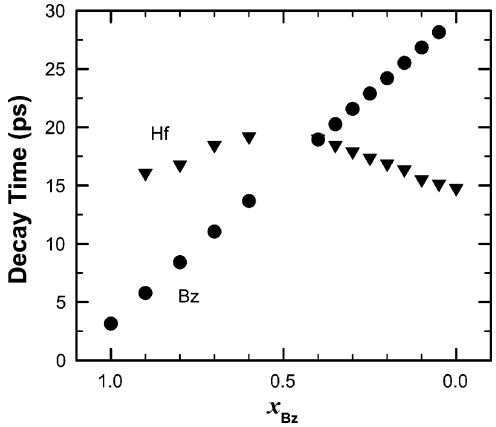

Figure 12. Experimental OKE decay times corresponding to benzene and hexafluorobenzene as a function of benzene mole fraction determined from nonlinear least-squares fits in which the benzene relaxation time was constrained to vary linearly with mole fraction.

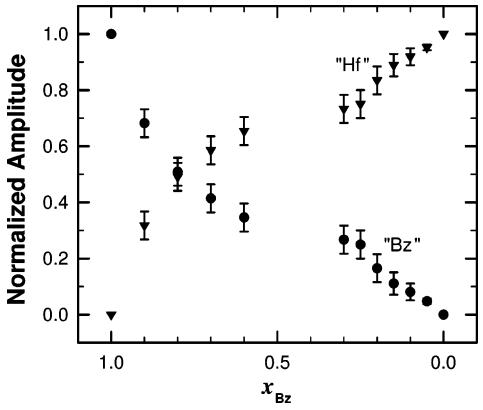

Figure 13. Experimental amplitudes corresponding to benzene and hexafluorobenzene as a function of benzene mole fraction determined from nonlinear least-squares fits in which the benzene relaxation time was constrained to vary linearly with mole fraction. The quotation marks in the labels denote that the amplitude of the more slowly relaxing component also contains the contribution of the coupling term.

The dependence of the amplitudes in Figure 13 on the benzene mole fraction is not a simple one, which gives us the opportunity to make an independent test of the validity of the fitting model we have used. The relative amplitudes of the components of the integrated OKE decay should be given by x_{Bz}^2, $[a_1(1 - x_{Bz})^2]$ and $[a_2 x_{Bz}(1 - x_{Bz})]$ for Bz−Bz, Hf−Hf, and Bz−Hf terms, respectively, where a_1 and a_2 are constants that must be determined. We have used these relations to try to reproduce the experimental amplitudes in Figure 13. The values of the parameters that yield the best fit are $a_1 = 2.5$ and $a_2 = 1.5$, and the resultant amplitudes are shown in Figure 14. While this model does not reproduce the amplitudes exactly, the correspondence is close enough to give us further support for the constrained fitting procedure used for the integrated OKE data.

We have also computed the ratios of collective-to-single-molecule relaxation times, τ_c^{aa}/τ_s^a, for all the liquids studied.

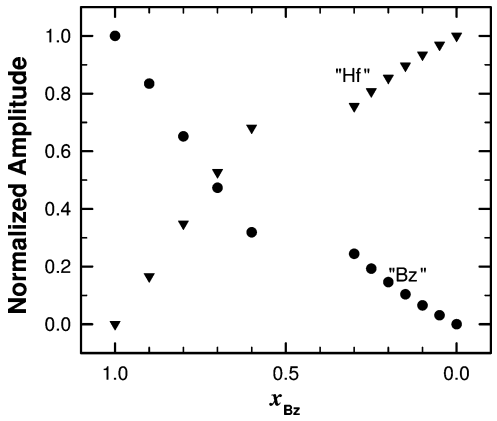

Figure 14. Calculated amplitudes corresponding to benzene and hexafluorobenzene as a function of benzene mole fraction using the parameters $a_1 = 2.5$ and $a_2 = 1.5$. The quotation marks in the labels denote that the amplitude of the more slowly relaxing component also contains the contribution of the coupling term.

Experimental values for collective and single-molecule reorientational times are available for the pure liquids and are also shown in Table 2. Experimental reported ratios τ_c/τ_s for the pure liquids are smaller than our computed values, corresponding to 1.05 for benzene and 1.32 for hexafluorobenzene.[58] As seen in Table 2 for the case of pure liquids, the estimations for single-molecule orientational relaxation times from MD simulations are closer to the experimental values than those for collective orientational times: our integrated values of τ_c are 28% and 75% larger than the experimental values for benzene and hexafluorobenzene, respectively, while the relative difference between experimental and computed values for τ_s lie around 3−8%. We believe that the discrepancy between theory and experiment in the collective relaxation times can be attributed to the known tendency of the Williams potential to overestimate the intermolecular interactions. Even though we have reduced the dispersive attractions between H and F atoms by rescaling the combination rule for cross H−F potential parameters, to get a good agreement with the experimental excess energy of mixing, it seems that it still predicts a slower rotational diffusive dynamics for the collective modes in these liquid mixtures. Indeed, even though the use of the Williams potential has demonstrated to predict satisfactorily well many thermodynamic and structural properties of the liquid phase in single component liquids and mixtures,[6,20,35] we should keep in mind that it has been originally developed and parametrized for simulations in the solid phase. Thus, some care must be taken in comparing experimental data and simulation results as it stands. However, we were able to extract interesting trends in the dynamic features from the simulations that are comparable with those exhibited by experiments.

Table 2 displays also the correlation times associated with the coupling term $\psi_{ab}^{MM}(t)$, which exceed somewhat the longer of the two collective times associated with like-molecule orientational TCFs.

Second Rank Orientational Correlation Factors. In single-component systems, the static second rank orientational pair correlation factor that describes the correlations between molecular anisotropic polarizability components is defined as the initial value of the molecular TCF,[29,59,65]

$$g_2 = \langle(\Pi_{xz}^{M})^2\rangle/\Gamma^2 = \psi_{xz}^{MM}(0) \tag{28}$$

In the rotational-diffusion limit, the single-molecule orientational TCF for symmetric top molecules decays exponentially, characterized by a relaxation time τ_s, and the collective orientational function is also exponential with a relaxation time τ_c; these times are related by

$$\tau_c = \left(\frac{g_2}{j_2}\right)\tau_s \tag{29}$$

where j_2 is a dynamic orientational correlation parameter. In the absence of orientational pair correlations, g_2 should be equal to unity (see eqs 15−17); the greater the tendency for local parallel or antiparallel ordering, the larger the value of $\langle P_2[\hat{\mathbf{u}}_i\cdot\hat{\mathbf{u}}_j]\rangle$ for $i \neq j$, and thereby of g_2.

In the case of binary mixtures of components *a* and *b*, additional static orientational pair correlation factors may be defined

$$g_2^{aa} = \frac{\langle(\Pi_{xz}^{M,a})^2\rangle}{\Gamma_a^2} = \frac{\Gamma^2}{\Gamma_a^2}\psi_{aa}^{MM}(0) \tag{30}$$

and

$$g_2^{ab} = \frac{\langle\Pi_{xz}^{M,a}\,\Pi_{xz}^{M,b}\rangle}{\Gamma^2} = \frac{1}{2}\,\psi_{ab}^{MM}(0) \tag{31}$$

Using the above definitions, g_2^{aa} should be equal to 1 if the pair correlations between like molecules are not taken into account (see eqs 15−17).

Values of g_2^{Bz-Bz}, g_2^{Hf-Hf} and g_2^{Bz-Hf} correlations computed from MD simulations are given in Table 3 for each mixture, along with experimental reported values for pure benzene and hexafluorobenzene. In much of the literature, j_2 is assumed to be equal to unity for pure liquids. Under this assumption, g_2 is equal to the ration τ_c/τ_s. We have tested the accuracy of the assumption $j_2 \approx 1$ for liquid acetonitrile and chloroform, at room temperature, obtaining values of $j_2 = 0.999$ and 1.009, respectively. Details of the potential models employed in the simulations of acetonitrile and chloroform can be found in ref 32.

Experimental values reported for g_2 of neat benzene lie in the range 0.78−1.16, while for neat hexafluorobenzene the reported range g_2 is wider, 1.4−2.75.[58,66,68−71] Our computed values for g_2 in neat liquids are within the range of experimental data.

As seen in Table 3, g_2^{Bz-Bz} increases with decreasing benzene concentration, in the same way as g_2^{Hf-Hf} decreases progressively when more Bz molecules are added to the liquid, and the Hf−Hf intraspecies correlations become weaker. These average values correspond to angles of ∼60° between Bz−Bz molecular planes for pure benzene and to ∼45° when the benzene mole fraction is reduced to 0.2. For Hf−Hf pairs, the variation of the angle between molecular symmetry axes lies in the range 35−45°, the latter value corresponds to the Bz-rich mixture and the former one to pure hexafluorobenzene. The

TABLE 3: Static Second Rank Orientational Pair Correlation Factors

x_{Bz}	g_2^{Bz-Bz}	g_2^{Hf-Hf}	g_2^{Bz-Hf}	g_2
1.0	0.918			0.918
Expt.				0.78−1.16[b]
0.8	0.980	1.259	0.197	1.469
0.5	1.126	1.376	0.317	1.929
0.2	1.254	1.377	0.203	1.769
0.0		1.509		1.509
Expt.				1.4[c]−2.75[b]

[a] Reference 68. [b] Reference 69. [c] Reference 58.

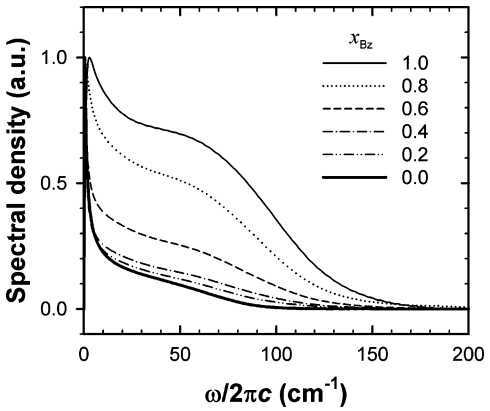

Figure 15. Normalized experimental OKE spectra as a function of benzene mole fraction.

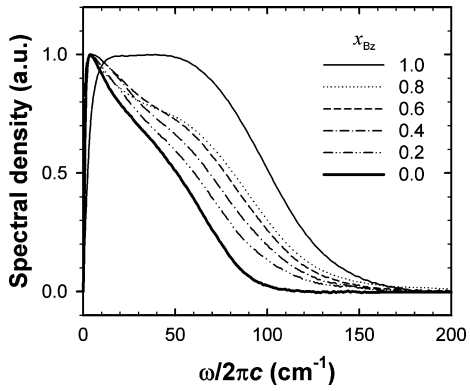

Figure 16. Normalized experimental OKE reduced spectral densities as a function of benzene mole fraction.

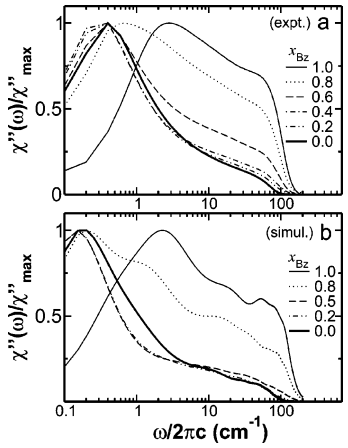

Figure 17. Normalized OKE spectra for mixtures, (a) from experiments and (b) from MD simulations, within the SS model. Benzene mole fractions are indicated in the figure. Note log scale on *x* axis.

cross Bz−Hf orientational static correlation, $g_2^{\mathrm{Bz-Hf}}$, has its maximum value at the equimolar composition, revealing a strong tendency for parallel ordering of unlike molecular pairs. As a net result, the total value of g_2 increases, until it reaches the maximum value for the benzene mole fraction of $x_{\mathrm{Bz}} = 0.5$.

By comparing the values of τ_c^{aa}/τ_s^a in Table 2 to those of g_2 in Table 3 for the pure liquids, it is possible to estimate the dynamical correlation factor, j_2. Using the relationship given by eq 29, we obtain $j_2 \approx 0.7$ for both pure liquids. Bauer et al.[58] estimated j_2 from depolarized Rayleigh scattering experiments in benzene and hexafluorobenzene by measuring the static correlation factor as the integrated intensities and the single-particle relaxation time by a different method (e.g., NMR relaxation or Raman band shapes). Using the relationship between the ratio τ_c/τ_s and g_2, they obtained dynamic correlation factors of $j_2 = 0.8$ and 1.06 for benzene and hexafluorobenzene, respectively. The static correlation factors reported in that work[58] are $g_2 = 0.80$ for benzene and $g_2 = 1.40$ for hexafluorobenzene, in good agreement with our computed values (see Table 3). Hence, we conclude that the poor agreement between theory and experiments for the dynamic correlation factor in hexafluorobenzene is due mainly to the much longer collective relaxation time obtained from MD simulations, probably originating in an overestimation of intermolecular interactions in our model potential, as already mentioned. Even though the collective times shown in Figure 11b are larger than those obtained by fitting the experimental OKE nuclear response by factors larger than 2 in the worst case, the experimental trend is qualitatively reproduced. We should also keep in mind that the values of the relaxation times shown in Figure 11 were obtained by an integration over time of the corresponding normalized TCF, while the experimental times shown in Figure 12 are the fitting parameters obtained from the long time behavior of the integrated experimental response function $R(t)$. We have chosen to estimate the relaxation times by time integrals of the TCFs because the simulated correlation functions arising from molecular polarizabilities of benzene and hexafluorobenzene intraspecies components $[\psi_{aa}^{\mathrm{MM}}(t)]$ were always better fitted by using a sum of two exponentials instead of a single exponential function. Hence, these characteristic times might not be directly comparable.

3. Kerr Spectra of Mixtures. It is also informative to examine the optical Kerr effect data in the frequency domain. Normalized OKE spectra at selected benzene mole fractions are shown in Figure 15, and the corresponding normalized reduced spectral densities (i.e., with the reorientational diffusion component removed) are shown in Figure 16. The reduced spectral densities of the neat liquids can both roughly be described as consisting of a high-frequency band and a low-frequency band. However, considering that the quadrupole moments and polarizabilities of benzene and hexafluorobenzene are similar, the reduced spectral densities are remarkably different. The entire hexafluorobenzene spectrum is shifted to lower frequency, as might be expected based on moment of inertia considerations. However, the lower-frequency feature is far more prominent in the hexafluorobenzene data. This low-frequency feature becomes evident upon the addition of a small mole fraction of hexafluorobenzene to benzene. We have noted previously that in neat liquids the intermediate response time tracks the collective orientational correlation time.[24] As we have seen above, the addition of a minority fraction of hexafluorobenzene to benzene increases the orientational correlation time of both components, and a corresponding increase in the respective intermediate response times is likely to be at least partly responsible for the rapid growth of the feature at low frequency. Thus, based on analogy with effects observed in neat liquids, any nonadditive effects in the orientational correlation times of the components of a mixture would be expected to extend to the intermediate response, and therefore cause nonadditive effects in the reduced spectral density as well.

In Figure 17 we compare, on a semilogarithmic scale, the normalized OKE spectra for mixtures from experiment and simulation. Even though the position of the diffusive peaks are slightly shifted toward smaller frequencies in the simulated OKE spectra $\chi''(\omega)$, the overall trend is well reproduced by the model.

When more Hf molecules are added to the liquid, the diffusive peak shifts toward smaller frequencies. The orientational diffusive dynamics is very sensitive to the amount of solvent

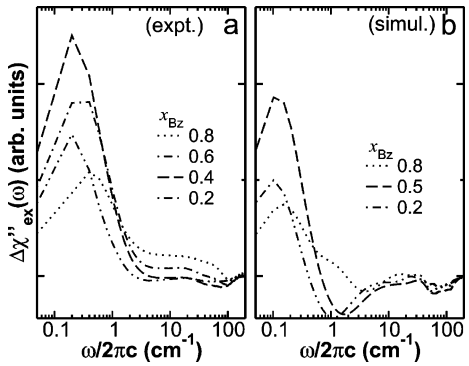

Figure 18. Excess OKE spectra of mixing, (a) from experiments and (b) from MD simulations, within the SS model.

displaced upon rotation; due to the increase in the number of strong and localized Bz−Hf interactions within the liquid, the effect of association between unlike species generates Bz−Hf complexes that move roughly twice as much solvent on rotation as the individual monomers.[58] Hence, the reorientational time of the complex should be slower than that of the monomers. As a consequence, in the frequency domain, the diffusive band should be shifted toward lower frequencies, as observed.

The role of interspecies interactions in the OKE response for mixtures can be qualitatively assessed by computing the excess spectrum of mixing, $\Delta\chi''_{ex}(\omega)$. We should first write the OKE susceptibility as a sum of two terms,

$$\chi''(\omega) = \chi''_{id}(\omega) + \Delta\chi''_{ex}(\omega) \tag{32}$$

with

$$\chi''_{id}(\omega) = x_{Bz}\,\chi''_{Bz}(\omega) + (1 - x_{Bz})\,\chi''_{Hf}(\omega) \tag{33}$$

where $\chi''_{Bz}(\omega)$ and $\chi''_{Hf}(\omega)$ are the OKE spectra for neat benzene and hexafluorobenzene, respectively. The right-hand side of eq 33 represents the weighted sum corresponding to a hypothetical ideal reference state in which interspecies interactions are absent. The excess term $\Delta\chi''_{ex}(\omega)$ measures the degree to which the data deviates from the additive ideal response, $\chi''_{id}(\omega)$. Analogous additivity relationships have been used to analyze the role of interspecies interactions of far IR spectra and OKE response of Bz−Hf mixtures.[9,10] Excess OKE spectra of mixing are shown in Figure 18.Both the experimental and simulated excess OKE spectra exhibit the largest deviations from additivity at low frequencies and for a benzene mole fraction near or equal to 0.5. Good qualitative agreement is found between experimental and simulated excess OKE spectra. Deviations from additivity occur mainly in the low-frequency region of the spectra, for $\omega/2\pi c < 5$ cm^{-1}. The excess OKE spectrum $\Delta\chi''_{ex}(\omega)$ exhibits a narrow band centered at about $\omega/2\pi c = 0.20-0.50$ cm^{-1} from experimental data, while the excess band is located at about 0.15 cm^{-1} in the simulated spectra. Both the experimental and simulated excess susceptibility peaks have a bandwidth of about ∼0.5−1 cm^{-1}, which correspond to time scales of the order of 30−60 ps; these times, in turn, are of the same order of magnitude as the times found for the estimations of lifetimes for Bz−Hf complexes in binary liquid mixtures,[20] from MD trajectories. The intensity of the peak increases and shifts toward lower frequencies with the dilution of benzene, until the equimolar composition in the simulated spectra and $x_{Bz} = 0.4$ from experiments are reached; revealing a strong nonideal behavior at those compositions. Such excess OKE spectrum is observed in a spectral range close to that of the OKE spectrum of neat hexafluorobenzene.

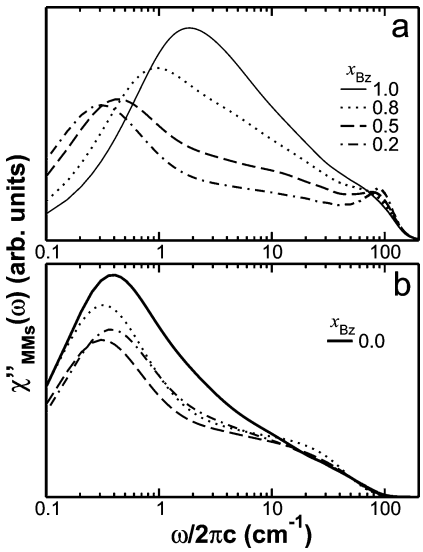

Figure 19. Single-molecule orientational contributions to OKE spectra for mixtures, from benzene (a) and hexafluorobenzene (b) molecules. Data were taken from normalized single-molecule TCFs, $\psi_{xz}^{MMs}(t)/\psi_{xz}^{MMs}(0)$.

Single-molecule correlations are substantially affected by interspecies interactions at intermediate and long times, as seen in Figure 10. Thus, their role on the change of the OKE spectrum upon mixing can be analyzed in the frequency domain, by studying the contribution from single-molecule susceptibilities to the OKE spectra, plotted in Figure 19.

In Figure 19a, a bimodal character can be observed in the single-molecule orientational spectra of benzene species in mixtures. A broad low-frequency band is observed in the spectra, that shifts from ∼2 cm^{-1} to ∼0.3 cm^{-1} going from neat benzene to $x_{Bz} = 0.2$; and a second and smaller peak is also present, showing up at $\omega/2\pi c \sim 100$ cm^{-1}, becoming visible with the addition of Hf molecules into the liquid. Our analysis suggests that the higher frequency peak corresponds to small amplitude orientational motions of benzene molecules relative to the first coordination shell of neighbors, whereas the lower frequency peak would stem from the motions of the Bz−Hf complex as a whole, under the influence of the remaining surrounding molecules. The enhancement of the intensity in the peak at ∼100 cm^{-1} with dilution, for the benzene single-molecule spectrum, indicates a higher restriction in the reorientation of the symmetry axis and a more hindered dynamics of benzene molecules within the liquid when the benzene mole fraction is reduced in the liquid.

The shift of the low-frequency peak in the single-molecule spectral susceptibility toward smaller frequencies when more Hf molecules are added to the liquid is consistent with the interpretation of that band as arising from reorientations of Bz−Hf complexes, given that those heterodimers should have slower tumbling dynamics than single Bz molecules. Moreover, the low-frequency peaks for benzene mole fractions of 50% and 20% are centered at a frequency similar to the corresponding peaks of the single-molecule orientational spectrum of pure hexafluorobenzene, shown also in Figure 19b.

The bimodal character in Hf single-molecule orientational spectrum seems to be much less pronounced than in Bz, though weak and flat shoulder can be observed at frequencies around 20 cm^{-1} for the mixtures. This reduction in the intensity in the high-frequency band for Hf, as compared to the case of Bz, is expected based on the larger moments of inertia of hexafluorobenzene, considering that the fourth moment in the expansion

of $\psi^{MMs}(t)$ at short times depends linearly on the mean square torque but inversely on the square moment of inertia (see eq 25). The ratio between the Hf and Bz moments of inertia corresponds to $I_\perp(Hf)/I_\perp(Bz) \approx 6$. Even though the forces among Hf molecules should be more intense than those among Bz molecules, based on the values of the potential parameters in Table 1, the potential does not seem to predict an increase by a factor of 36 in the mean square torque on the symmetry axis of Hf molecules, otherwise the intensities of the high-frequency band in $\chi''_{MMs}(\omega)$ should be comparable to those for benzene. The low-frequency maximum in Hf does not change very much its position with composition, staying centered around 0.4 cm^{-1} for the range of concentrations studied.

While the intensity of the global maximum for the Bz curves in Figure 19a decreases monotonically from pure benzene to the Hf-rich mixture, those corresponding to Hf curves in panel (b) of Figure 19 show a decrease in the intensity going from pure hexafluorobenzene until the equimolar mixture is reached, and then the maximum increases again at $x_{Bz} = 0.8$. This change in the intensities reflects the behavior already observed in the relaxation rate of the corresponding single-molecule orientational function $\psi^{MMs}(t)$ as a function of the benzene mole fraction.

VI. Concluding Remarks

We have studied the relaxation dynamics of the collective polarizability anisotropy in liquid mixtures of benzene and hexafluorobenzene of different compositions at room temperature, by Raman-induced Kerr effect experiments and MD simulations. The simulated polarizability response arising from intermolecular interactions was included using the first-order DID model and calculated considering both molecule-centered and distributed site polarizabilities, the latter resulting in closer agreement with experimental data.

We found good qualitative agreement between experiments and theory for the overall behavior of the nuclear response function and susceptibility as a function of composition. Namely, we observed that the location of the inertial maximum in the nuclear response function shifts toward longer times as more Hf molecules are added to the liquid; their long time diffusive decay rates decrease with the addition of molecules of the other kind into the mixture when compared with those in the corresponding single-component liquids, due to the formation of strong and localized associations between Bz and Hf species that hinder the rotational diffusive dynamics; and the orientational correlation times (arising from collective and single-molecule modes) obtained for Bz species was observed to increase monotonically with decreasing benzene mole fraction, while those for Hf species increases with the addition of Bz molecules until the point the two mole fractions are similar, exhibiting a maximum peak near $x_{Bz} = 0.5$. By analyzing the computed molecular time correlation function $\psi^{MM}_{xz}(t)$ in terms of its three contributions arising from benzene, hexafluorobenzene and the coupling between the two species, we saw that there is an important contribution of the latter to the total intensity of molecular correlations. The coupling term also causes the total molecular TCF to decay more slowly than the sum of Bz−Bz and Hf−Hf molecular correlations. The orientational correlation time associated with the molecular coupling term was always the most slowly decaying molecular component, and its decay rate was numerically close to that of the slowest intraspecies component. Therefore, the parameters obtained from the fitting of the experimental integrated nuclear response function with a sum of two exponentials can still be interpreted as the orientational correlation times associated to benzene and hexafluorobenzene, taking into account that those correlation times also contain contributions from the slow Bz−Hf correlations. It will be interesting to see if this behavior is universal in strongly associating liquid mixtures.

MD simulations allowed us to reproduce the trends that emerge from experiments for the polarizability anisotropy relaxation, although the quantitative comparison with OKE experimental data was not as satisfactory, resulting in collective orientational relaxation times that are larger by a factor of ∼2 than those inferred from the fittings of the OKE experimental signals to biexponential functions at long times. We attribute the numerical discrepancy to the use of the Williams potential, as already mentioned. Even though we have reduced the dispersive attractive interactions between H and F atoms in order to get good agreement with the experimental excess energy of mixing, by rescaling the combination rule for H−F cross potential parameters, the potential model still seems to overestimate the intermolecular interactions and thus it predicts not only a slower translational dynamics, but also a slower rotational diffusion dynamics than in the real fluid. It could also be likely that solid-like structures persist in the simulated fluids because the MD simulations have been carried out at room temperature, which is rather close to the melting point of the binary mixture.

Both the OKE experiments and MD simulation results support the presence of strongly associated complexes in solution that remain bound over time scales significantly longer than that of a typical molecular collision. A rough estimation from the inverse bandwidth of the excess OKE spectrum of mixing would indicate that the lifetimes of these interspecies complexes lie in the range of 30−60 ps, in agreement with previous estimations from MD simulations.[20]

In view of the slow dynamics predicted by the Williams potential, we believe that it would be worth making a systematic study in order to obtain a new set of potential parameters that is able to reproduce the transport properties and the characteristic times associated to translational and rotational dynamics in closer agreement with the available experimental data. These calculations are currently under way.

Acknowledgment. This work was supported by the National Science Foundation, grants CHE-0073228 and CHE-0314020 (J.T.F.) and CHE 9981539 (B.M.L.). J.T.F. is Research a Corporation Cottrell Scholar and a Camille Dreyfus Teacher-Scholar.

References and Notes

(1) Patrick, C. R.; Prosser, G. S. *Nature* **1960**, *187*, 1021.
(2) Overell, J. S. W.; Pawley, G. S. *Acta Crystallogr.* **1982**, *B38*, 1966.
(3) Williams, J. H.; Becucci, M. *Chem. Phys.* **1993**, *177*, 191.
(4) Gaw, W. J.; Swinton, F. L. *Trans. Faraday Soc.* **1968**, *64*, 2023.
(5) Bartsch, E.; Bertagnolli, H.; Chieux, P. *Ber. Bunsen-Ges. Phys. Chem.* **1986**, *90*, 34.
(6) Cabaço, M. I.; Danten, Y.; Besnard, M.; Guissani, Y.; Guillot, B. *J. Phys. Chem. B* **1998**, *102*, 10712.
(7) Smith, N. A.; Meech, S. R. *Int. Rev. Phys. Chem.* **2002**, *21*, 75.
(8) Chang, Y. J.; Castner, E. W., Jr. *J. Chem. Phys.* **1993**, *99*, 113.
(9) Tassaing, T.; Danten, Y.; Besnard, M.; Zoïdis, E.; Yarwood, J. *Chem. Phys.* **1994**, *184*, 225.
(10) Neelakandan, M.; Pant, D.; Quitevis, E. L. *Chem. Phys. Lett.* **1997**, *265*, 283.
(11) Tanabe, K.; Hirashi, J. J. *Raman Spectrosc.* **1982**, *12*, 274.
(12) Chelli, R.; Cardini, G.; Ricci, M.; Bartolini, P.; Righini, R.; Califano, S. *Phys. Chem. Chem. Phys.* **2001**, *3*, 2803.
(13) Ryu, A.; Stratt, R. M. *J. Phys. Chem. B* **2004**, *108*, 6782.
(14) Smith, N. A.; Lin, S. J.; Meech, S. R.; Shirota, H.; Yoshihara, K. *J. Phys. Chem. A* **1997**, *101*, 9578.
(15) Smith, N. A.; Lin, S. J.; Meech, S. R.; Yoshihara, K. *J. Phys. Chem. A* **1997**, *101*, 3641.
(16) Chang, Y. J.; Castner, E. W. *J. Phys. Chem.* **1996**, *100*, 3330.

(17) McMorrow, D.; Lotshaw, W. T. *Chem. Phys. Lett.* **1993**, *201*, 369.
(18) Rajian, J. R.; Hyun, B. R.; Quitevis, E. L. *J. Phys. Chem. A* **2004**, *108*, 10107.
(19) Neelakandan, M.; Pant, D.; Quitevis, E. L. *J. Phys. Chem. A* **1997**, *101*, 2936.
(20) Elola, M. D.; Ladanyi, B. M. *J. Chem. Phys.* **2005**, *123*, Art. No. 224508.
(21) Farrer, R. A.; Loughnane, B. J.; Deschenes, L. A.; Fourkas, J. T. *J. Chem. Phys.* **1997**, *106*, 6901.
(22) Scodinu, A.; Fourkas, J. T. *J. Phys. Chem. B* **2002**, *106*, 10292.
(23) McMorrow, D.; Lotshaw, W. T. *Chem. Phys. Lett.* **1991**, *178*, 69.
(24) Loughnane, B. J.; Scodinu, A.; Farrer, R. A.; Fourkas, J. T.; Mohanty, U. *J. Chem. Phys*. **1999**, *111*, 2686.
(25) McMorrow, D.; Lotshaw, W. T. *J. Phys. Chem.* **1991**, *95*, 10395.
(26) McMorrow, D. *Opt. Commun*. **1991**, *86*, 236.
(27) Ladanyi, B. M.; Liang, Y. Q. *J. Chem. Phys*. **1995**, *103*, 6325.
(28) Frenkel, D.; McTague, J. P. *J. Chem. Phys*. **1980**, *72*, 2801.
(29) Paolantoni, M.; Ladanyi, B. M. *J. Chem. Phys*. **2002**, *117*, 3856.
(30) Thole, B. T. *Chem. Phys.* **1981**, *59*, 341.
(31) van Duijnen, P. T.; Swart, M. *J. Phys. Chem. A* **1998**, *102*, 2399.
(32) Elola, M. D.; Ladanyi, B. M. *J. Chem. Phys.* **2005**, *123*, 224506; Note that the expression following eq 7 in this article should read $\mathbf{\Pi} = \mathbf{\Pi}^{M,\bar{\alpha}} + \mathbf{\Pi}^{M,\gamma} + \mathbf{\Pi}^{I,\bar{\alpha}\bar{\alpha}} + \mathbf{\Pi}^{I,\bar{\alpha}\gamma} + \mathbf{\Pi}^{I,\gamma\gamma}$.
(33) Williams, D. E.; Cox, S. R. *Acta Crystallogr*. **1984**, *B40*, 404.
(34) Williams, D. E.; Houpt, D. *J. Acta Crystallogr*. **1986**, *B42*, 286.
(35) Cabaço, M. I.; Danten, Y.; Besnard, M.; Guissani, Y.; Guillot, B. *J. Phys. Chem. B* **1997**, *101*, 6977.
(36) Borin, I. A.; Skaf, M. S. *J. Chem. Phys*. **1999**, *110*, 6412.
(37) Song, W.; Rossky, P. J.; Maroncelli, M. *J. Chem. Phys.* **2003**, *119*, 9145.
(38) Dantzler Siebert, E. M.; Knobler, C. M. *J. Phys. Chem.* **1971**, *75*, 3863.
(39) Duncan, W. A.; Sheridan, J. P.; Swinton, F. L. *Trans. Faraday Soc.* **1966**, *62*, 1090.
(40) Hogenboom, D. L.; Krynicki, K.; Sawyer, D. W. *Mol. Phys.* **1980**, *40*, 823.
(41) Ciccotti, G.; Ferrario, M.; Ryckaert, J. P. *Mol. Phys*. **1982**, *47*, 1253.
(42) Verlet, L. *Phys. Rev.* **1967**, *159*, 98.
(43) Allen, M. P.; Tildesley, D. J. *Computer Simulation of Liquids*; Oxford University Press: New York, 1994.
(44) Ryckaert, J. P.; Ciccotti, G.; Berendsen, H. J. C. *J. Comput. Phys.* **1977**, *23*, 327.
(45) Alms, G. R.; Burnham, A. K.; Flygare, W. H. *J. Chem. Phys*. **1975**, *63*, 3321.
(46) Gentle, I. R.; Ritchie, G. L. D. *J. Phys. Chem.* **1989**, *93*, 7740.
(47) Mossa, S.; Ruocco, G.; Sampoli, M. *J. Chem. Phys.* **2002**, *117*, 3289.
(48) Chelli, R.; Cardini, G.; Procaci, P.; Righini, R.; Califano, S.; Albrecht, A. *J. Chem. Phys.* **2000**, *113*, 6851.
(49) Smith, N. A.; Meech, S. R. *J. Phys. Chem. A* **2000**, *104*, 4223.
(50) Hattori, T.; Terasaki, A.; Kobashahi, T.; Wada, T.; Yamada, A.; Sasabe, H. *J. Chem. Phys.* **1991**, *95*, 937.
(51) Friedman, J. S.; Lee, M. C.; She, C. Y. *Chem. Phys. Lett.* **1991**, *186*, 161.
(52) Fourkas, J. T. *Ultrafast Infrared and Raman Spectroscopy*; Fayer, M. D. Ed.; Marcel Dekker: New York, 2001.
(53) Bartolini, P.; Ricci, M.; Torre, R.; Righini, R. *J. Chem. Phys*. **1999**, *110*, 8653.
(54) Ricci, M.; Bartolini, P.; Chelli, R.; Cardini, G.; Califano, S.; Righini, R. *Phys. Chem. Chem. Phys*. **2001**, *3*, 2795.
(55) Califano, S.; Righini, R.; Walmsley, S. H. *Chem. Phys. Lett*. **1979**, *64*, 491.
(56) Lynden-Bell, R. M.; Steele, W. A. *J. Phys. Chem.* **1984**, *88*, 6514.
(57) Skaf, M. S.; Vechi, S. M. *J. Chem. Phys.* **2003**, *119*, 2181.
(58) Bauer, D. R.; Brauman, J. I.; Pecora, R. *J. Chem. Phys.* **1975**, *63*, 53.
(59) Stassen, H.; Dorfmüller, T.; Ladanyi, B. M. *J. Chem. Phys*. **1994**, *100*, 6318.
(60) Gordon, R. G. *J. Chem. Phys.* **1965**, *43*, 1307.
(61) St. Pierre, A.; Steele, W. A. *Mol. Phys*. **1981**, *43*, 123.
(62) McQuarrie, D. A. *Statistical Mechanics*; Harper & Row: New York, 1976.
(63) Wang, K. S.; Yuan, P.; Schwartz, M. *Spectrochim. Acta* **1993**, *49A*, 1035.
(64) Fischer, J.; Weiss, A. *Ber. Bunsen-Ges. Phys. Chem.* **1986**, *90*, 1141.
(65) Madden, P. A.; Tildesley, D. *J. Mol. Phys*. **1985**, *55*, 969.
(66) Kivelson, D.; Madden, P. A. *Annu. Rev. Phys. Chem*. **1980**, *31*, 523.
(67) Jannelli, M. P.; Magazu, S.; Migliardo, P.; Aliotta, F.; Tettamanti, E. *J. Phys.: Condens. Matter* **1996**, *8*, 8157.
(68) Vrbancich, J.; Ritchie, G. L. D. *Chem. Phys. Lett*. **1983**, *94*, 63.
(69) Battaglia, M. R.; Cox, T. I.; Madden, P. A. *Mol. Phys.* **1979**, *37*, 1413.
(70) Brown, N. M. D.; Maguire, J. F.; Swinton, F. L. *Faraday Discuss. Chem. Soc*. **1978**, 244.
(71) Burnham, A. K.; Alms, G. R.; Flygare, W. H. *J. Chem. Phys*. **1975**, *62*, 3289.